HHS Public Access

Author manuscript

J Magn Reson Imaging. Author manuscript; available in PMC 2016 December 01.

Published in final edited form as:

J Magn Reson Imaging. 2015 December ; 42(6): 1747–1758. doi:10.1002/jmri.24941.

Increased speed and image quality in single shot fast spin echo imaging via variable refocusing flip angles

Andreas M. Loening, MD, PhD[1], **Manojkumar Saranathan, PhD**[1], **Nichanan Ruangwattanapaisarn, MD**[1,2], **Daniel V. Litwiller, PhD**[3], **Ann Shimakawa, MS**[4], and **Shreyas S. Vasanawala, MD, PhD**[1]

[1]Department of Radiology, Stanford University School of Medicine, Stanford, CA, United States [2]Department of Diagnostic and Therapeutic Radiology, Ramathibodi Hospital, Mahidol University, Bangkok, Thailand [3]GE Healthcare Global MR Applications and Workflow, Rochester, MN, United States [4]GE Healthcare Global MR Applications and Workflow, Menlo Park, CA, United States

Abstract

Purpose—To develop and validate clinically a single shot fast spin echo (SSFSE) sequence utilizing variable flip angle refocusing pulses to shorten acquisition times via reductions in specific absorption rate (SAR) and improve image quality

Materials and Methods—A variable refocusing flip angle SSFSE sequence (vrfSSFSE) was designed and implemented, with simulations and volunteer scans performed to determine suitable flip angle modulation parameters. With IRB approval/informed consent, patients referred for 3T abdominal MRI were scanned with conventional SSFSE and either half-Fourier (n=25) or full-Fourier vrfSSFSE (n=50). Two blinded radiologists semi-quantitatively scored images on a scale from −2 to 2 for contrast, noise, sharpness, artifacts, cardiac-motion related signal loss, and the ability to evaluate the pancreas and kidneys.

Results—vrfSSFSE demonstrated significantly increased speed (~2-fold, $p<0.0001$). Significant improvements in image quality parameters with full-Fourier vrfSSFSE included increased contrast, sharpness, and visualization of pancreatic and renal structures with higher bandwidth technique (mean scores 0.37, 0.83, 0.62, and 0.31, respectively, $p\leq0.001$), and decreased image noise and improved visualization of renal structures when used with equal bandwidth technique (mean scores 0.96 and 0.35, respectively, $p<0.001$). Increased cardiac-motion related signal loss with full-Fourier vrfSSFSE was seen in the pancreas but not the kidney.

Conclusion—vrfSSFSE increases speed at 3T over conventional SSFSE via reduced SAR, and when combined with full-Fourier acquisition can improve image quality although with some increased sensitivity to cardiac-motion related signal loss.

Keywords

single shot fast spin echo; variable refocusing flip angle; specific absorption rate; echo stabilization

Corresponding Author: Andreas M. Loening, MD, PhD, address: 300 Pasteur Dr, H1307 MC 5621, Stanford, CA 94305, work: (650) 498-3878, fax: (650) 723-1909, loening@stanford.edu.

INTRODUCTION

As one of the most basic contrast mechanisms in magnetic resonance imaging, T2-weighted imaging is integral to the majority of MRI protocols. Currently, T2-weighted imaging is most often accomplished with fast spin echo (FSE) sequences. FSE sequences generally require several minutes of acquisition time for each scan plane orientation, and are challenging in body imaging due to motion. Although periodic motion can be compensated for using several techniques (respiratory triggering, gating, etc. (1,2)), these approaches further increase scan times, suffer from a lack of robustness, and fail to compensate for non-periodic sources of motion such as irregular breathing and bowel peristalsis.

The strongest candidate for replacing conventional T2-weighted FSE sequences in body imaging has been single shot fast spin echo (SSFSE), also known as half Fourier acquisition single shot turbo spin echo (HASTE). SSFSE largely retains the T2-weighting and robustness to field inhomogeneity of FSE, while adding speed and relative robustness to motion as each image is acquired within a single echo train. In its current implementation, the major limitations of SSFSE compared to FSE has been its reduced signal-to-noise ratio due to reduced acquisition time, as well as blurring and reduced image contrast due to T2-decay occurring during the extended echo train (3).

In the absence of specific absorption rate (SAR) considerations and T2 decay, the ideal pulse sequence for SSFSE would consist of a 90° excitation pulse followed by a train of 180° refocusing pulses. In practice SAR considerations place limits on the refocusing flip angles used at higher field strengths for both FSE and SSFSE, and at 3T a constant train of 130° pulses is often utilized. The use of refocusing pulses less than 180° introduces a degree of T1 weighting, but as T1 is much greater than T2 for most biologic tissues and its relative variation is less, the T1 contribution to signal intensity can be effectively ignored (4). Even for 130° refocusing pulses, the SSFSE repetition rate is limited by SAR considerations, and speed improvements and/or coverage improvements for multiple slice SSFSE can be made by further reducing the refocusing flip angles (4). A caveat to this approach is that at lower flip angles a greater amount of the signal acquired arises from stimulated echoes built up over the echo train, and this increases sensitivity to motion induced signal loss (5,6).

Utilizing variable refocusing flip angles instead of a constant refocusing flip angle, a method utilized extensively in 3D-FSE (7), can stabilize the signal amplitude over the course of the echo train. For a properly designed variable flip angle train, much of the initial magnetization can be stored in the longitudinal direction at the beginning of the echo train, and can then be slowly converted back to transverse magnetization to stabilize the amplitude of the acquired signal. Stabilizing the level of transverse magnetization over the acquisition reduces T2-decay related modulation of the acquired signal, thereby reducing blurring that would otherwise manifest in the phase encoding direction. Additionally, incorporating lower flip angles at the beginning of the echo train serves to slow the effective rate of T2 relaxation (4,8), allowing image contrast to reflect a shorter effective echo time than what would be expected from the timing of when the center of k-space is acquired in relation to the initial excitation pulse.

Multiple methods have previously been suggested for generating variable refocusing flip angle echo trains to reduce SAR and/or maintain signal over the image acquisition (4,8–11). These approaches have previously been implemented for 2D-FSE, b-SSFP, half-Fourier SSFSE imaging, and most extensively for 3D-FSE (7). The method of Busse *et al*. (8,9), developed for 3D-FSE imaging and applied to the case of SSFSE imaging in this work, conveniently parameterizes the variable refocusing flip angle train as a set of 4 control points suitable for parameter optimization.

SSFSE is generally performed utilizing half-Fourier technique (half-NEX). This is done to reduce the echo train length due to SAR considerations, as well as to allow clinically relevant echo times to be achieved as T2 contrast is largely determined by the time duration between the initial excitation pulse and the echo at which the center of k-space is acquired. For a full-Fourier (full-NEX) SSFSE acquisition utilizing a conventional constant refocusing flip angle, the effective echo time achieved would be too long to generate clinically useful T2-weighted contrast for most applications, and the additional echo train length would lead to SAR limitations further increasing the slice repetition time (TR). Given the effective T2-decay prolongation ability of a properly designed variable flip angle refocusing train along with its greatly reduced SAR, full-Fourier SSFSE imaging with clinically relevant effective echo times should be achievable.

Thus, current SSFSE imaging consists of somewhat blurred images that are acquired relatively inefficiently due to SAR constraints imposing long inter-slice gaps. In this work, we implemented a variable refocusing flip angle approach for single shot fast spin echo imaging, determined a suitable set of parameters describing the refocusing flip angle train, and assessed for both half and full-Fourier acquisitions the resulting impact on imaging speed, sharpness, noise, and other image quality features.

MATERIALS AND METHODS

vrfSSFSE Sequence

The variable refocusing flip angle approach described by Busse *et al*. (8) was implemented for the case of single shot fast spin echo imaging and termed vrfSSFSE (variable refocusing flip-angle SSFSE). Four control angles (α_{init}, α_{min}, α_{cent}, $\alpha_{last)}$ are utilized for specifying the refocusing flip angle train with smooth modulation between these parameters. Starting from α_{init} (fixed at 130° for all experiments), the refocusing flip angles are ramped down to α_{min} (flip angle at echo = 6), ramped up to α_{cent} (flip angle used when the center of k-space is acquired), and then ramped up or down to α_{last} (flip angle at end of echo train). Example echo trains are shown in FIGURE LEGENDS Figure 1A. As there are large echo-to-echo changes in signal intensity in the beginning of the echo train, the first 4 echoes were discarded in all cases to allow signal levels to stabilize. The use of low flip angles at the beginning of the train reduces the effective T2 relaxation rate and maintains a steady signal level, decreasing image blurring (8). It has been shown that these control angles determine the signal modulation (and hence point spread function/blurring) as well as influence image contrast, signal-to-noise ratio (SNR) and SAR (8).

A half-sinc radiofrequency (RF) pulse option was also implemented, in which the side-lobes of the RF pulse were removed to decrease the RF transmission time (12). This option, combined with interleaved slice acquisition, was utilized when full-Fourier vrfSSFSE imaging was performed to allow shorter effective echo times via reduced echo spacing.

Computation of Effective TE

Due to the mixing of stimulated and spin echoes and effective prolongation of T2-decay, the generated image contrast does not directly reflect the echo time (TE) at which the center of k-space is acquired. To generate a contrast-equivalent echo time (TE_{eff}), the method of Busse *et al.* (9) was implemented. In this method, the annotated TE_{eff} approximately represents the image contrast that would be generated by a spin echo technique with a 180° refocusing pulse. This method requires an estimate of the T1/T2 relaxation times of the tissue being imaged. Prior work has shown that for solid organs within the abdomen and pelvis at 3T, T2 relaxation times range between approximately 40–120 ms and T1 relaxation times range between approximately 700–1600 ms (13). Target values of T1=1600 ms and T2=60 ms were utilized in this work to roughly match the renal medulla. The exact choice of target values is somewhat arbitrary, as previous work has shown that the computation of TE_{eff} is relatively stable across a range of T1/T2 values (7,9). Note that for a given echo train length the desired effective echo time may not be directly achievable. This is most noticeable with half-Fourier vrfSSFSE, where the T2-decay prolongation properties stemming from the reduced refocusing flip angles entails that shorter requested echo times can require additional echoes to be inserted prior to traversing the center of k-space. These additional echoes can either be discarded, or incorporated into the k-space data to generate additional signal, but result in a longer total echo train length increasing the repetition time.

Parameter Optimization

An extended phase graph (EPG) algorithm was implemented in MATLAB (MathWorks, MA) and used to simulate the effect of the three control angle parameters α_{min}, α_{cent}, and $\alpha_{last.}$ While the signal was parameterized using these control angles in Busse *et al.* (9), it was never carefully optimized, especially for SAR and minimum TR, which was our goal. For the simulations, representative soft tissue T1 and T2 values of 1600 ms and 60 ms, respectively, were used (13). A rectangular object was modeled and the k-space profile of the object multiplied by the signal modulation from the EPG simulation for a given refocusing flip angle train. This modulated profile was then Fourier-transformed, and the mean signal amplitude at the center of the object was used to obtain the signal intensity. Relative SAR was computed as the sum of the square of the refocusing flip angles divided by the echo train length. The sequence TR, which is the maximum of the TR determined by the length of the echo train and the SAR limited TR, was determined by entering the sequence parameters into the MRI console assuming an 85 kg subject. Scanning was performed on a volunteer (38 yrs, 85 kg, male) to confirm the simulation results and allow subjective image assessment using both half-Fourier and full-Fourier techniques, and was performed with the same parameters utilized for the subsequent clinical testing described below.

Clinical Testing

Clinical testing was performed with IRB approval and informed consent. Adult patients referred for abdominal MRI examinations were recruited into one of three groups: comparison of conventional SSFSE and half-Fourier vrfSSFSE for renal/adrenal indications, comparison of conventional SSFSE and full-Fourier vrfSSFSE for renal/adrenal indications, and comparison of conventional SSFSE and full-Fourier vrfSSFSE for pancreatic indications. Consecutive patients were utilized, and there were no exclusion criteria. Patient characteristics are shown in Table 1. Patients were scanned on a 3.0T MRI scanner (MR750, GE Healthcare, Waukesha, WI) using a 32-channel torso coil and an ARC parallel imaging factor 3. Each subject was imaged with conventional SSFSE (constant refocusing flip angle of 130°, half-Fourier) and vrfSSFSE (either half- or full-Fourier), with all parameters kept as identical as achievable. Scan parameters are shown in Table 1. For conventional SSFSE and half-Fourier vrfSSFSE sequences, k-space filling was performed with homodyne reconstruction. Effective TE was set to 100–130 ms, or if this was not obtainable as low as possible. Field of view was optimized to each patient's anatomy (28–48 cm), but was kept within 2-cm between both sequences for a given subject. Acquisition plane was coronal to match current imaging protocols utilizing SSFSE at our institution.

Imaging Grading

A semi-quantitative grading system using pre-determined criteria was utilized that judged noise, contrast, sharpness, general artifacts, cardiac motion related signal loss artifacts over the pancreas or kidney, and the ability to diagnose pancreatic or renal abnormalities, on a scale from −2 to 2 (Table 2). Both the pancreas and kidney were evaluated for all cases independent of whether the examination was performed for pancreatic or renal/adrenal indications. Two readers (SSV and AML with 8 years and 1 year of experience interpreting body MRI, respectively) independently scored each pair of images (conventional SSFSE versus vrfSSFSE) in a blinded, randomized order, with a non-blinded assistant utilized to transcribe the scores. SNR measurements were obtained by region of interest (ROI) analysis, with SNR calculated as the mean signal of the tissue ROI divided by the standard deviation of the noise ROI. For each pair of images (conventional SSFSE versus vrfSSFSE), tissue ROI's were drawn by one of the authors (AML, 15 years experience with medical imaging analysis) over the tissue of interest taking care to avoid areas with artifacts and intra-parenchymal vessels. ROI size and placement were identical between each pair of images, with a minimum ROI size of 1 cm. The noise ROI's were similarly identically sized and placed between each image pair, but drawn over areas of extracorporeal air. Contrast to noise (CNR) measurements were calculated as the absolute difference between the mean signal of two different tissue ROI's divided by the standard deviation of the noise ROI.

Statistics

For the semi-quantitative imaging grading, the null hypothesis of no significant difference in image quality between sequences was assessed with a Wilcoxon signed rank test, with two-tailed $p<0.05$ considered statistically significant with a Holm-Bonferroni correction for multiple comparisons (14). Inter-observer variability was assessed utilizing a Weighted Cohen's kappa statistic. Difference in SNR, CNR, repetition time (utilized as a proxy for

scan time), and TE_{eff}, were assessed with the null hypothesis of no significant difference using Student's two-tailed paired t-test with $p<0.05$ considered statistically significant and a Holm–Bonferroni correction for multiple comparisons.

RESULTS

Parameter Optimization

Rather than maintaining transverse magnetization over long echo trains as was done in Busse *et al*. (8), we explored the flip angle parameter space with the goal of minimizing TR/SAR while maintaining SNR and contrast. The three control parameters used to determine the refocusing flip angle train and, hence, the signal behavior, were α_{min}, α_{cent}, and α_{last} (α_{init} was fixed at 130° throughout as in (8)).

Optimization of α_{min}—Lowering α_{min} produced a flatter signal response (FIGURE LEGENDS Figure 1B), but required longer echo trains in the half-Fourier case to achieve the desired TE_{eff} at the center of k-space, increasing the minimum TR (Figure 2A). For the half-Fourier case a value of $\alpha_{min} = 90°$ yielded the minimum TR limited only by echo train length (as opposed to SAR limited TR) (Figure 2A). This value was also optimal for SNR as the signal was relatively insensitive to α_{min} for a fixed value of TE_{eff}. (Figure 2B).

Optimization of α_{cent}—With α_{min} at the optimal value, decreases in α_{cent} were shown to cause decreases in both SAR and normalized signal (Figure 2C). Prioritizing signal over SAR, we set the optimal value of α_{cent} at 100°. In practice, we found that the TR with $\alpha_{cent} = 100°$ was not SAR limited when combined with the other parameters chosen.

Optimization of α_{last}—From simulations (Figure 2D) and preliminary volunteer scanning (not shown) we found that signal appeared relatively insensitive to α_{last}, which was set to 45° for all experiments to minimize SAR/TR.

These optimal parameters were fairly insensitive to T1/T2 of the basic tissue types (liver, endometrium, renal cortex and medulla), as has previously been described (9). We also performed simultaneous optimization of these three flip angle variables instead of one at a time to ensure global minima and a complete search of the parameter space (results omitted for clarity).

For the half-Fourier variable refocusing flip angle acquisition, the effective T2-decay prolongation could be inefficient for longer effective echo times (> 100 ms) or low α_{min} values (< 90°), as the signal from multiple refocusing echoes would need to be discarded while waiting for the effective T2 decay to evolve to the point that the center of k-space could be acquired for the desired TE_{eff}. One approach to make use of these echoes is to extend the coverage on the under-sampled portion of k-space. We decided to utilize the effective T2-prolongation properties of the variable refocusing flip angle method to achieve full k-space coverage (full-Fourier). For full-Fourier simulations lower α_{min} values yielded flatter signal responses (FIGURE LEGENDS Figure 1B), but was also important for achieving more clinically appropriate effective echo times. Taking into consideration motion

related signal loss (discussed below), an α_{min} of 60° was utilized that could achieve 120–130 ms TE_{eff}.

Scanning of a volunteer was utilized to verify the results of the simulations. What was not modeled in the simulations was that decreasing α_{min} resulted in increasing susceptibility to motion related signal loss. For moderate values of α_{min} (60–100°) this manifested predominantly as cardiac motion related signal loss over the left lobe of the liver (Figure 3), and was intermittent depending upon the relative timing of the pulse sequence and the cardiac cycle (6). For lower values of α_{min} (50° or less) larger areas of signal loss occurred, again predominantly due to cardiac motion but respiratory motion effects could also be seen if acquisitions were performed during free-breathing.

Half-Fourier vrfSSFSE Clinical Scanning

Conventional SSFSE was directly compared to half-Fourier vrfSSFSE for renal and adrenal clinical indications. A representative example is shown in Figure 4. The half-Fourier vrfSSFSE acquisition was twice as fast as conventional SSFSE at 3T (Figure 5A), with a mean TR of 619 ms versus 1221 ms for half-Fourier vrfSSFSE versus conventional SSFSE, respectively. The images were analyzed utilizing a semi-quantitative scoring system (Table 2), and no significant differences were identified in the assessed imaging characteristics (Figure 5B, all p-values > 0.025 and non-significant after correcting for multiple comparisons).

The Weighted Cohen's kappa statistic for all observations in the conventional SSFSE versus half-Fourier vrfSSFSE comparison was 0.47, indicating moderate agreement between the two readers (15). The average TE_{eff} was 100 ms for conventional SSFSE and 103 ms for half-Fourier vrfSSFSE, while this difference was significant ($p<0.001$) it was of small magnitude and unlikely to be clinically relevant. SNR estimates derived from ROI analysis demonstrated small but significant 18% ($p=0.0005$) and 12% ($p=0.006$) decreases in SNR with half-Fourier vrfSSFSE compared to conventional SSFSE for the liver and spleen, respectively (Figure 6A). SNR differences in other assessed organs were not significant (all remaining p-values > 0.01 and non-significant after correcting for multiple comparisons). CNR estimates demonstrated a significant 28% increase ($p=0.004$) with half-Fourier vrfSSFSE compared to conventional vrfSSFSE for pancreas versus kidney (Figure 6B).

Full Fourier vrfSSFSE Clinical Scanning

Conventional SSFSE was directly compared to full-Fourier vrfSSFSE for renal/adrenal and pancreatic clinical indications. Examples of the acquired images are shown in Figure 7 and Figure 8. The full-Fourier vrfSSFSE acquisition was demonstrated to be more than twice as fast as conventional SSFSE at 3T (Figure 5A); for renal/adrenal cases the mean TR was 568 ms versus 1320 ms, and for pancreas cases 587 ms versus 1323 ms, for full-Fourier vrfSSFSE versus conventional SSFSE, respectively. For the renal/adrenal cases utilizing equal bandwidth in both techniques (Figure 5B), vrfSSFSE showed a significant decrease in image noise (mean score 0.96, $p<0.0001$) and a significant increase in the visualization of renal structures (mean score 0.35, $p<0.001$). For the pancreatic cases in which conventional SSFSE utilized lower bandwidth (Figure 5B), vrfSSFSE showed a significant increase in

image contrast (mean score 0.37, p=0.0001) and sharpness (mean score 0.83, p<0.0001), a small but significant decrease in artifacts (mean score 0.23, p=0.002), as well as a significant increase in the visualization of pancreatic (mean score 0.62, p=0.0003) and renal structures (mean score 0.31, p=0.001). In both cases, vrfSSFSE showed a significant increase in cardiac motion related signal loss occurring over the pancreas (mean score −0.52 and −0.35 for renal/adrenal and pancreas cases, respectively, p<0.0005). The Weighted Cohen's kappa statistic for all observations in the conventional SSFSE versus full-Fourier vrfSSFSE comparison was 0.59, indicating moderate agreement between the two readers (15). For renal/adrenal cases, the average TE_{eff} was 130 ms for conventional SSFSE and 133 ms for full-Fourier vrfSSFSE, this difference was not significant (p=0.08). For pancreatic cases, the average TE_{eff} was 121 ms for conventional SSFSE, and 130 ms for full-Fourier vrfSSFSE, this difference was significant (p<0.01). For the renal/adrenal cases (Figure 6A), SNR estimates derived from ROI analysis demonstrated significant increases (≥18%) in SNR for all assessed tissue types (all p values <0.0003). For the pancreas cases (Figure 6A), SNR estimates demonstrated a small but significant 17% decrease in SNR for liver (p=0.005) and 13% increase in SNR for muscle (p=0.006), with differences in other assessed organs not significant (remaining p values >0.08). CNR estimates (Figure 6B) demonstrated a significant increase with full-Fourier vrfSSFSE in renal/adrenal cases compared to conventional vrfSSFSE for both liver versus spleen (50%, p<0.0001) and pancreas versus kidney (57%, p=0.001), and a significant increase with full-Fourier vrfSSFSE in pancreas cases compared to conventional vrfSSFSE for liver versus spleen (37%, p=0.015).

DISCUSSION

In abdominal MRI, T2-weighted imaging utilizing fast-spin echo sequences is fraught with artifacts stemming from periodic and non-periodic motion, leading to attempts to replace FSE with single shot fast spin echo imaging. In this work we have presented a new SSFSE sequence utilizing an echo train with variable refocusing flip angles, which improves on conventional SSFSE by achieving shorter scan times and, when combed with full-Fourier acquisition, better image quality.

Both the half-Fourier and the full-Fourier vrfSSFSE implementations showed imaging speed improvements of at least two-fold compared to conventional SSFSE under the conditions tested. Long breath holds can be taxing for many clinical patients due to underlying cardiopulmonary disease or deconditioning. These speed improvements reduce the breath-hold time by half for the same number of slices, or enable twice as many images to be acquired in the same breath hold time. For the example of a standard clinical case utilizing 32 slices to cover the upper abdomen, this acquisition would require a 40 s breath hold using conventional SSFSE, and only 20 s when utilizing vrfSSFSE.

This improvement in image acquisition time is a direct reflection of the reduced refocusing flip-angles utilized in this variable flip angle technique. SSFSE imaging is particularly SAR constrained at 3T, and is artificially slowed down in order to stay within regulatory constraints for the deposition of radiofrequency energy in the human body. Much of the improvement we saw in decreasing SAR/improving the imaging acquisition time reflected decreasing the flip angles utilized toward the end of the echo train. We utilized an α_{last} of

45° in our echo train, while conventional SSFSE utilized a constant flip angle of 130°. The simulations demonstrated that an equivalent amount of signal could be obtained at the end of the echo train with a low flip angle while greater reducing SAR.

In practice, we found that for strictly half-Fourier k-space coverage setting α_{min} to below 90° was not optimal from a repetition time perspective due to the effective T2-decay prolongation. In order to reach our target effective echo time of 100 ms when using an α_{min} below 90°, this T2-prolongation necessitated the acquisition of additional echoes prior to traversing the center of k-space beyond that typically needed for overscanning in half-Fourier techniques. Although not explored in this study, rather than being discarded these extra echoes could be utilized to fill additional lines in k-space to achieve an acquisition with between half and full-Fourier k-space coverage. In this work we instead used the T2-prolongation to allow full-Fourier k-space coverage with vrfSSFSE, and optimized our refocusing flip angle train to achieve clinical relevant effective echo times.

One potential pitfall of using reduced refocusing flip angles is the increased sensitivity to motion related signal loss, particularly cardiac related motion manifested predominantly as bulk signal loss over the left lobe of the liver (16). This artifact is thought to be due to the lower flip angles leading to longer refocusing pathways, thereby creating a longer time period over which phase shifts from motion can accumulate (5,6). For the half-Fourier case with α_{min} set to 90°, the cardiac motion related signal loss was negligible for imaging the pancreas or kidneys. For the full-Fourier case, the trade-off between α_{min} values became more complicated. Lowering α_{min} allowed clinically relevant effective echo times to be reached (< 140 ms), but resulted in increasing cardiac motion related signal loss that effected a larger region of the upper abdomen. Empirically, we found that an α_{min} of 60° was the best trade-off between these two constraints, yielding an effective echo times of ~130 ms without changing other scan parameters, and preserving visualization of most upper abdominal organs.

We semi-quantitatively evaluated conventional SSFSE compared to both half-Fourier vrfSSFSE and full-Fourier vrfSSFSE in routine clinical cases. The pancreas and kidneys were specifically examined to evaluate the tradeoffs between cardiac motion related signal loss and diagnostic capabilities in the upper abdomen. For the half-Fourier vrfSSFSE comparison there were no significant differences in the assessed parameters. Although increased signal loss over the left lobe of the liver due to cardiac motion was intermittently seen, this artifact did not extend to the kidneys or pancreas in the half-Fourier vrfSSFSE case.

For the full-Fourier vrfSSFSE comparison, the kidneys were still well enough separated from cardiac motion that there were no appreciated disadvantages to using full-Fourier vrfSSFSE for their evaluation, and there was a significant improvement in visualization of renal structures. In the case of the pancreas, there was a significant increase in the intermittently present cardiac motion related signal loss over this organ for the full-Fourier vrfSSFSE sequence. Despite this artifact, the readers judged the vrfSSFSE images to be better for evaluation of pancreatic structures, and we anticipate that it will be a matter of personal preference as to which sequence will be preferred by other institutions.

In the full-Fourier vrfSSFSE comparisons, there were slightly different parameters between the pancreatic and renal/adrenal cases in that the conventional SSFSE utilized in pancreatic cases used a lower bandwidth (±83 kHz) than that utilized for full-Fourier vrfSSFSE (±125 kHz), while in the renal/adrenal cases the bandwidth was equivalent (±125 kHz). The results of the semi-quantitative analysis reflect this difference. When equivalent bandwidth was utilized full-Fourier vrfSSFSE was judged to have a significant decrease in noise compared to conventional SSFSE. When decreased bandwidth was utilized for the conventional SSFSE, full-Fourier vrfSSFSE was judged to have equivalent noise but improved contrast and sharpness. These improvements are consistent with increased signal being available with the full-Fourier vrfSSFSE acquisition, and are anticipated both due to the decrease in T2-signal modulation with the variable refocusing flip angle technique as well as from more lines in k-space being acquired instead of synthesized.

Quantitative measurements of signal to noise and contrast to noise are complicated in the setting of acceleration (17). We performed ROI based estimations of SNR and CNR, and while the absolute values of these measurements will be biased as has been previously described in the literature, the relative changes in SNR and CNR between the conventional SSFSE and its paired vrfSSFSE sequence should remain a valid comparison as aside from the refocusing flip angle train all other parameters were maintained as constant as possible. In the renal/adrenal cases, full-Fourier vrfSSFSE demonstrated small significant increases in SNR relative to conventional SSFSE in all tissue types. This was felt to reflect predominantly the differences in bandwidth between the two sequences as discussed above. In the pancreas cases, full-Fourier vrfSSFSE had a small but significant difference in liver SNR compared to conventional SSFSE. This could have arisen from two effects. First, the vrfSSFSE sequences had a significantly longer TE_{eff} than the conventional SSFSE sequences in the pancreas cases. Second, confounding vascular signal in the conventional SSFSE sequence may have biased the SNR measurement, as vrfSSFSE demonstrated more intrinsic flow suppression in vessels. Given the issues with quantitative assessment of SNR and CNR in the setting of acceleration, we lend more weight to the semi-quantitative image quality results performed with criteria focused on image quality features that are clinically relevant.

There are several points that remain to be explored regarding vrfSSFSE. The cardiac motion related signal loss appears to be the major caveat to this technique in the upper abdomen, but we anticipate this could be ameliorated via the utilization of cardiac gating to correctly time the vrfSSFSE acquisition during the quiescent portion of the cardiac cycle. In this work we focused on the abdomen, but we anticipate that even greater clinical improvements can be made in pelvic imaging where cardiac motion will not be a limitation, and we are targeting future work to evaluate the diagnostic trade-off for replacing FSE T2-weighted imaging in pelvic indications. Additionally, this work has focused entirely on imaging at 3T, as that is where our current clinical practice is largely focused. Although SSFSE imaging at 1.5T does not suffer from the same SAR constraints as imaging at 3T, we anticipate that the other advantages of utilizing a variable flip angle for SSFSE imaging will still manifest at 1.5T including T2-prolongation (allowing full-Fourier imaging) and decreased blurring.

There were several limitations to this study. First, as already discussed, SNR and CNR measurements are difficult when acceleration is employed, although the relative changes should remain valid. Second, due to our local use pattern for SSFSE imaging, assessment was only performed in the coronal plane, and results may not be directly generalizable to different imaging planes with different acceleration factors. Finally, the study evaluated differences in image quality and did not measure clinical impact. Although the image evaluation was performed by radiologists and included an assessment of perceived diagnostic capability, no measures were performed to assess whether perceived improvements yielded improvements in the final radiologic interpretation or other clinical outcomes.

In conclusion, we have implemented and clinically demonstrated a single shot fast spin echo sequence utilizing a variable refocusing flip angle echo train that doubles the speed of acquisition at 3T compared to conventional SSFSE. For the half-Fourier case, this new sequence demonstrated equivalent image quality for the assessed parameters. For the full-Fourier case, this new sequence demonstrated improved image quality compared to conventional SSFSE for evaluation of structures in the upper abdomen, but these improvements must be tempered by the increased sensitivity to intermittent cardiac motion related signal loss for structures that are close to the heart.

Acknowledgments

Grant Support:

- Tashia and John Morgridge Faculty Scholars Fund
- NIH R01EB009690

The authors would like to thank Lloyd Estkowski of GE Healthcare for helpful discussions and technical aid in implementing clinical protocols.

References

1. Chavhan GB, Babyn PS, Vasanawala SS. Abdominal MR imaging in children: motion compensation, sequence optimization, and protocol organization. Radiographics. 2013; 33:703–719. [PubMed: 23674770]
2. Yang RK, Roth CG, Ward RJ, deJesus JO, Mitchell DG. Optimizing abdominal MR imaging: approaches to common problems. Radiographics. 2010:185–199. [PubMed: 20083593]
3. Bhosale P, Ma J, Choi H. Utility of the FIESTA pulse sequence in body oncologic imaging: review. AJR Am J Roentgenol. 2009; 192:S83–93. [PubMed: 19458102]
4. Hennig J, Weigel M, Scheffler K. Multiecho sequences with variable refocusing flip angles: optimization of signal behavior using smooth transitions between pseudo steady states (TRAPS). Magn Reson Med. 2003; 49:527–535. [PubMed: 12594756]
5. Madhuranthakam, AJ.; Busse, RF.; Brittain, JH.; Rofsky, NM.; Alsop, DC. Sensitivity of low flip angle SSFSE of the abdomen to cardiac motion. Proceedings of the 15th Annual Meeting of ISMRM; Berlin, Germany. 2007; p. abstract 2523
6. Litwiller, DV.; Holmes, JH.; Saranathan, M., et al. Sensitivity of modulated refocusing flip angle single-shot fast spin echo to impulsive cardiac-like motion. Proceedings of the 22nd Annual Meeting of ISMRM; Milan, Italy. 2014; p. abstract 1613
7. Mugler JP 3rd. Optimized three-dimensional fast-spin-echo MRI. J Magn Reson Imaging. 2014; 39:745–767. [PubMed: 24399498]
8. Busse RF, Brau A, Vu A, et al. Effects of refocusing flip angle modulation and view ordering in 3D fast spin echo. Magn Reson Med. 2008; 60:640–649. [PubMed: 18727082]

9. Busse RF, Hariharan H, Vu A, Brittain JH. Fast spin echo sequences with very long echo trains: design of variable refocusing flip angle schedules and generation of clinical T2 contrast. Magn Reson Med. 2006; 55:1030–1037. [PubMed: 16598719]
10. Mugler, JP., 3rd; Kiefer, B.; Brookeman, JR. Three-dimensional T2-weighted imaging of the brain using very long spin-echo trains. Proceedings of the 8th Annual Meeting of ISMRM; Denver. 2000; p. abstract 687
11. Lichy MP, Wietek BM, Mugler JP 3rd, et al. Magnetic resonance imaging of the body trunk using a single-slab, 3-dimensional, T2-weighted turbo-spin-echo sequence with high sampling efficiency (SPACE) for high spatial resolution imaging: initial clinical experiences. Invest Radiol. 2005; 40:754–760. [PubMed: 16304477]
12. Bernstein, M.; King, K.; Zhou, X. Handbook of MRI Pulse Sequences. 1. Burlington: Elsevier Academic Press; 2004. p. 37-43.
13. de Bazelaire CM, Duhamel GD, Rofsky NM, Alsop DC. MR imaging relaxation times of abdominal and pelvic tissues measured in vivo at 3. 0 T: preliminary results. Radiology. 2004; 230:652–659. [PubMed: 14990831]
14. Holm S. A simple sequentially rejective multiple test procedure. Scand J Statist. 1979; 6:65–70.
15. Landis JR, Koch GG. The measurement of observer agreement for categorical data. Biometrics. 1977; 33:159–174. [PubMed: 843571]
16. Mannelli L, Wilson GJ, Dubinsky TJ, et al. Assessment of the liver strain among cirrhotic and normal livers using tagged MRI. J Magn Reson Imaging. 2012; 36:1490–1495. [PubMed: 22777877]
17. Dietrich O, Raya JG, Reeder SB, Ingrisch M, Reiser MF, Schoenberg SO. Influence of multichannel combination, parallel imaging and other reconstruction techniques on MRI noise characteristics. Magn Reson Imaging. 2008; 26:754–762. [PubMed: 18440746]
18. Lebel RM, Wilman AH. Intuitive design guidelines for fast spin echo imaging with variable flip angle echo trains. Magn Reson Med. 2007; 57:972–975. [PubMed: 17457879]

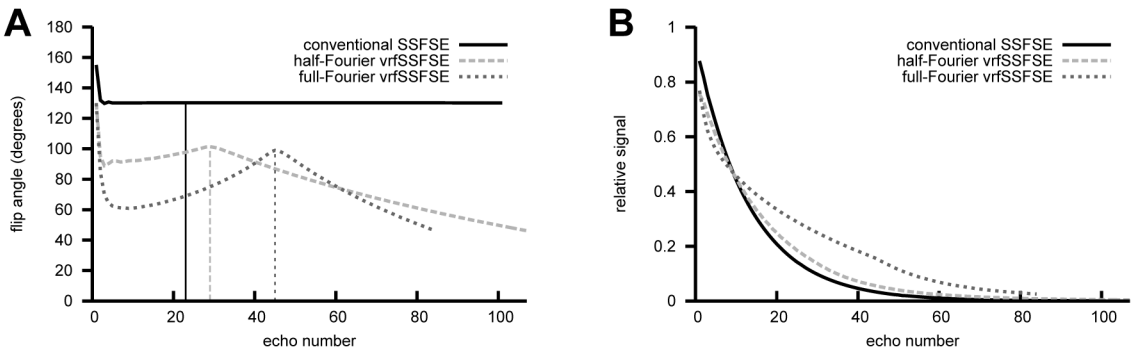

Figure 1.

(A) Example flip angle trains for conventional SSFSE ($\alpha = 130°$), half-Fourier vrfSSFSE ($\alpha_{init} = 130°$, $\alpha_{min} = 90°$, $\alpha_{cent} = 100°$, $\alpha_{last} = 45°$), and full-Fourier vrfSSFSE ($\alpha_{init} = 130°$, $\alpha_{min} = 60°$, $\alpha_{cent} = 100°$, $\alpha_{last} = 45°$). The vertical lines indicate where the center of k-space is traversed. Echo trains were generated to achieve an effective TE of 130 ms. The full-Fourier vrfSSFSE example has a shorter echo train as a smaller number of phase encodes were utilized in this example. (B) Corresponding simulated signal curves for the different echo trains, note the flattening of the signal curve for echo trains with decreased values of α_{min}.

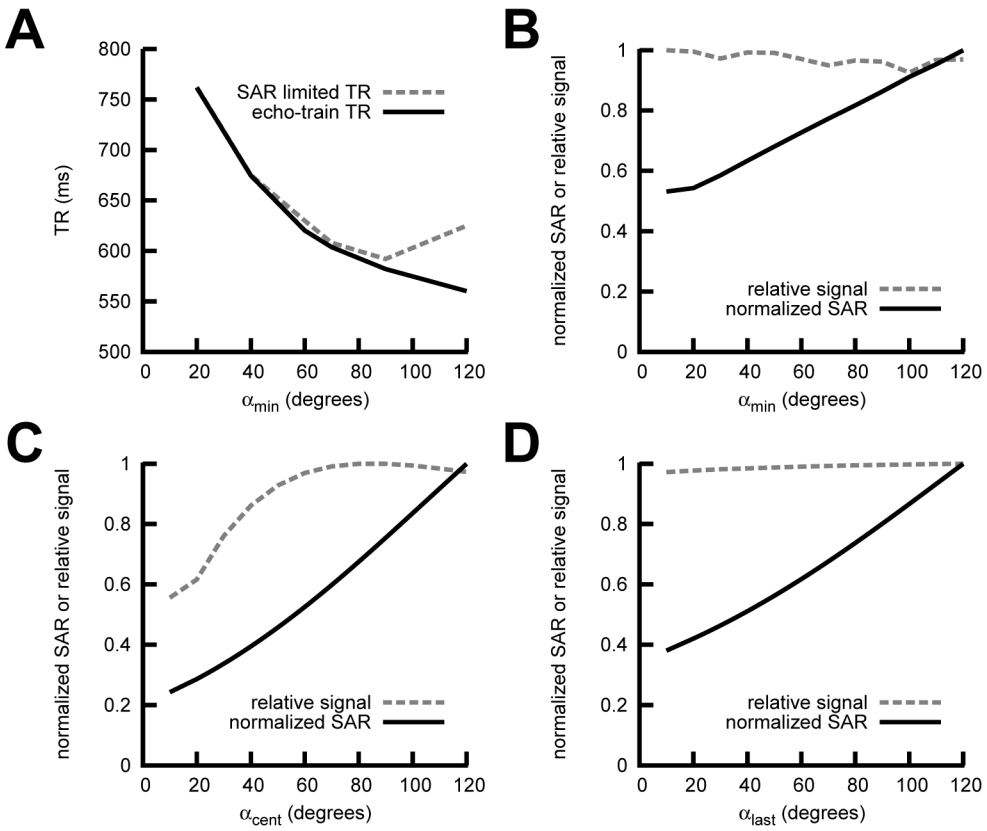

Figure 2.

Half-Fourier vrfSSFSE EPG Simulation Results. (A) Echo train length limited TR and specific absorption rate (SAR) limited TR vs. α_{min} for TE 100 ms. Normalized signal output and normalized SAR for (B) α_{min}, (C) $\alpha_{cent,}$ and (D) α_{last}. The non-varying parameters were α_{init}=130°, α_{min}=90°, α_{cent}=100°, and α_{last}=45°.

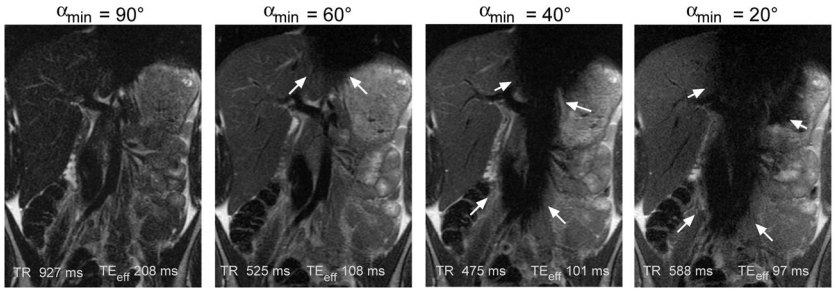

Figure 3.

Cardiac motion related signal loss for full-Fourier vrfSSFSE sequences with varying α_{min}. Representative slices are shown for the most severely affected slices, although this artifact (arrows) is intermittent presumably related to timing of acquisition relative to phase of the cardiac cycle. For higher α_{min} (e.g. 90°) and full-Fourier technique only a relatively long effective TE is obtainable (> 180 ms) resulting in low signal images. For lower α_{min} (e.g. < 50°) the artifact becomes overly problematic and compromises the diagnostic ability of the images.

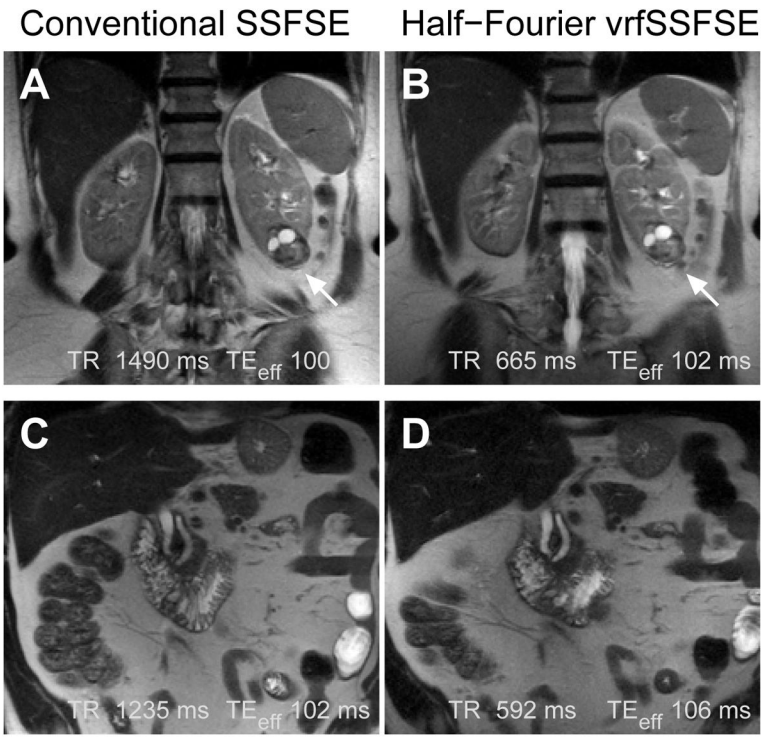

Figure 4.

Examples of conventional SSFSE compared to half-Fourier vrfSSFSE. (A) Conventional SSFSE and (B) half-Fourier vrfSSFSE images from a patient with renal cell carcinoma of the left kidney (arrow). (C) Conventional SSFSE and (D) half-Fourier vrfSSFSE images from a patient with a mildly dilated pancreatic and common bile duct. Images are mildly cropped from the full field of view. Note the equivalent image quality.

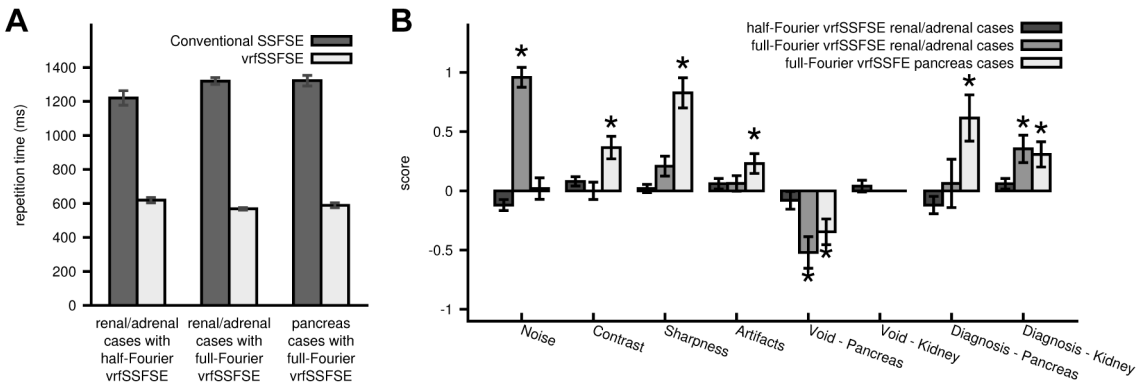

Figure 5.

Comparison of conventional SSFSE and vrfSSFSE. A: Comparison of repetition times (TR). For each pair (conventional SSFSE versus vrfSSFSE) the differences were significant ($p<0.0001$). B: Results of semi-quantitative grading for noise, contrast, sharpness, general artifacts, cardiac motion related signal loss over the pancreas and kidney, and the ability to diagnose pancreatic or renal abnormalities. * indicates significant differences. The scoring system utilized is explained in Table 2. Negative numbers favor conventional SSFSE, positive numbers favor vrfSSFSE. The presence/absence of a cardiac motion related signal void impacting the kidneys was not statistically evaluated in the full-Fourier vrfSSFSE cases, as it was not seen in any of the cases. Error bars are standard error of the mean.

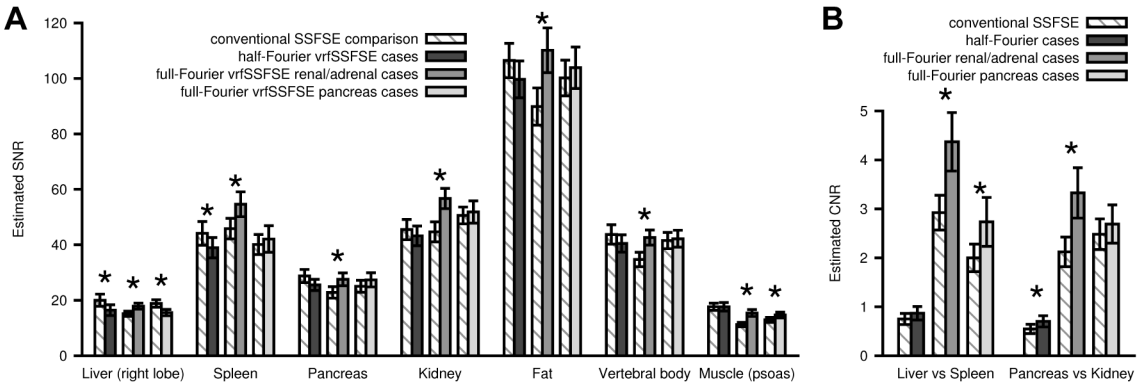

Figure 6.

Estimated signal to noise (SNR) and contrast to noise (CNR) based on clinical data. (A) SNR and (B) CNR are shown for half-Fourier vrfSSFSE renal/adrenal, full-Fourier vrfSSFSE renal/adrenal, and full-Fourier pancreas cases, adjacent to their comparison conventional SSFSE. SNR was calculated as mean signal in the tissue ROI divided by standard deviation from an ROI placed over extra-corporeal air. CNR was calculated as the absolute difference in signal for the two tissues divided by the standard deviation from an ROI placed over extra-corporeal air. * indicates significant differences between the conventional SSFSE and the corresponding vrfSSFSE sequence. Error bars are standard error of the mean.

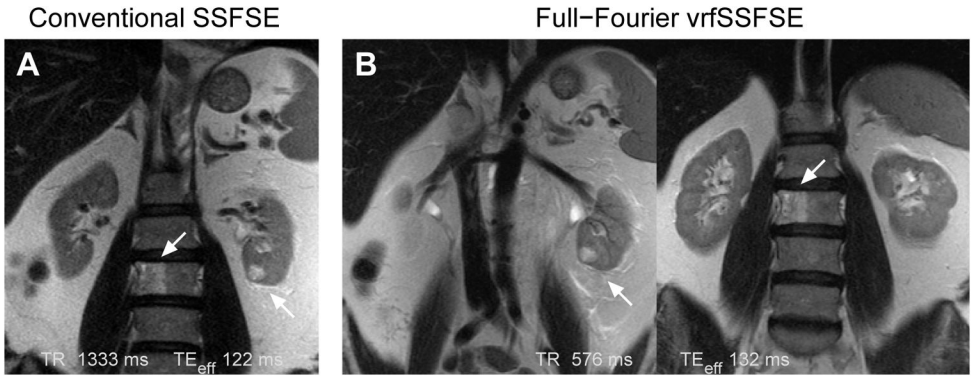

Figure 7.

Comparison of conventional SSFSE to full-Fourier vrfSSFSE for imaging of the kidney. (A) Conventional SSFSE image showing a renal cell carcinoma of the left kidney (right arrow) and an L3 vertebral body lesion that proved to be a hemangioma (left arrow). (B) Two images from the same full-Fourier vrfSSFSE acquisition showing the small renal cell carcinoma (left image) and the hemangioma (right image). Note the decreased noise compared to the conventional SSFSE image, and improved visualization of the characteristic vertical striations of the L3 vertebral body hemangioma. The differences in positioning are due to the conventional SSFSE needing to be acquired using respiratory triggering (images acquired at end-expiration). As the vrfSSFSE images can be acquired in half the time, the full stack of 38 images was acquired during a single 22 s breath hold. Images are moderately cropped.

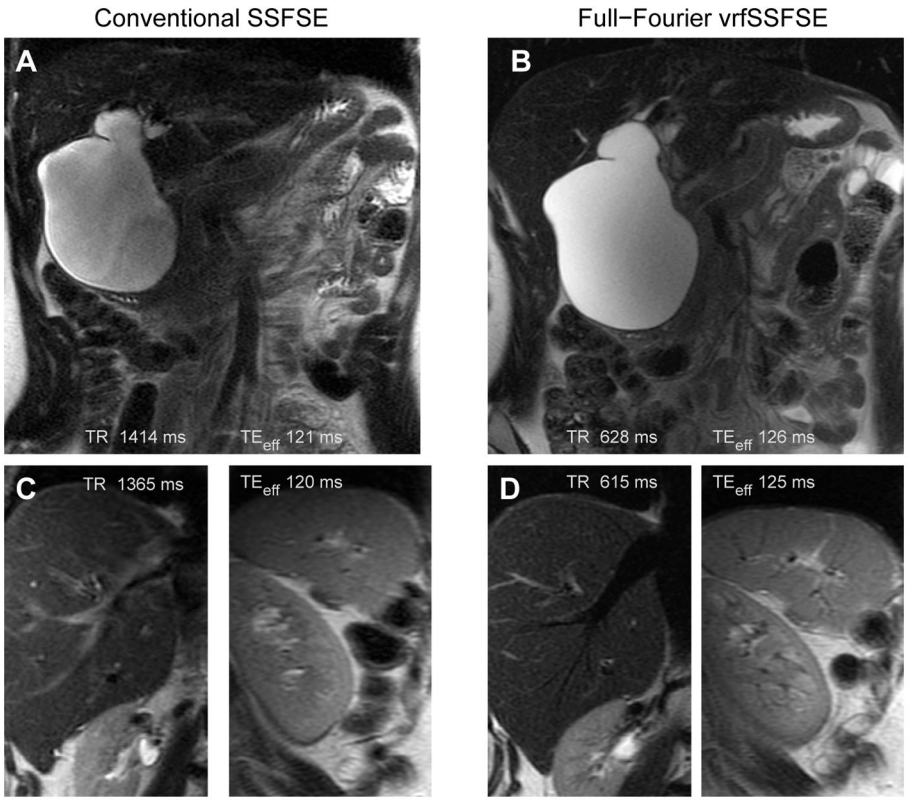

Figure 8.

Comparison of conventional SSFSE to full-Fourier vrfSSFSE acquired for evaluation of the pancreas and biliary ducts. (A) Conventional SSFSE and (B) full-Fourier vrfSSFSE images demonstrate a type I choledochocele that causes mass effect upon the pancreas as seen by the altered course of the pancreatic duct. Images are mildly cropped. Close up views from a different patient of the liver and spleen for (C) conventional SSFSE and (D) full-Fourier vrfSSFSE highlight the more prominent black blood appearance of vasculature with the vrfSSFSE technique. This is best seen in the hepatic vein in the liver and small branching vessels radiating from the hilum of the spleen.

Table 1

Scan and patient population parameters.

	Renal/Adrenal cases with half-Fourier vrfSSFSE		Renal/Adrenal cases with full-Fourier vrfSSFSE		Pancreas cases with full-Fourier vrfSSFSE	
	Conventional SSFSE	**vrfSSFSE**	**Conventional SSFSE**	**vrfSSFSE**	**Conventional SSFSE**	**vrfSSFSE**
refocusing flip angles	130°	α_{init} = 130° α_{min} = 90° α_{cent} = 100° α_{last} = 45°	130°	α_{init} = 130° α_{min} = 60° α_{cent} = 100° α_{last} = 45°	130°	α_{init} = 130° α_{min} = 60° α_{cent} = 100° α_{last} = 45°
bandwidth	±50 kHz	±50 kHz	±125 kHz	±125 kHz	±83 kHz	±125 kHz
matrix	416x320	416x320	416x256	416x256	416x256	416x256
slice thickness	5 mm	5 mm	5 mm	5 mm	4 mm	4 mm
acceleration	3	3	3	3	3	3
k-space coverage	half	half	half	full	half	full
patients recruited (male/female)	25 (12/13)		24 (15/9)		26 (12/14)	
age mean (range)	59 yrs (23–84)		58 yrs (21–89)		63 yrs (40–82)	

Table 2

Semi-quantitative scoring criteria utilized for conventional SSFSE versus vrfSSFSE evaluation.

	Favors SSFSE			Favors vrfSSFSE	
Score	**−2**	**−1**	**0**	**1**	**2**
Noise	SSFSE with decreased graininess with improved diagnostic capability	SSFSE with decreased graininess without diagnostic impact	Equivalent	vrfSSFSE with decreased graininess without diagnostic impact	vrfSSFSE with decreased graininess with improved diagnostic capability
Image Contrast	SSFSE with good contrast between liver/spleen **AND** renal cortex/ medulla not seen in vrfSSFSE	SSFSE with good contrast between liver/spleen **OR** renal cortex/medulla not seen in vrfSSFSE	Equivalent	vrfSSFSE with good contrast between liver/spleen **OR** renal cortex/medulla not seen in SSFSE	vrfSSFSE with good contrast between liver/spleen **AND** renal cortex/ medulla not seen in SSFSE
Sharpness	SSFSE with increased sharpness between renal cortex/fat **AND** renal cortex/medulla not seen in vrfSSFSE	SSFSE with increased sharpness between renal cortex/fat **OR** renal cortex/ medulla not seen in vrfSSFSE	Equivalent	vrfSSFSE with increased sharpness between renal cortex/fat **OR** renal cortex/ medulla not seen in SSFSE	vrfSSFSE with increased sharpness between renal cortex/fat **AND** renal cortex/medulla not seen in SSFSE
Artifacts (besides cardiac motion related non-uniformity)	SSFSE with decreased artifacts to the point of improved diagnostic capability	SSFSE with decreased artifacts without diagnostic impact	Equivalent	vrfSSFSE with decreased artifacts without diagnostic impact	vrfSSFSE with decreased artifacts to the point of improved diagnostic capability
Motion related non- uniformity over organ of interest - Pancreas	SSFSE with decreased artifacts to the point of improved diagnostic capability	SSFSE with decreased artifacts without diagnostic impact	Equivalent	vrfSSFSE with decreased artifacts without diagnostic impact	vrfSSFSE with decreased artifacts to the point of improved diagnostic capability
Motion related non- uniformity over organ of interest - Kidney/ Adrenal	SSFSE with decreased artifacts to the point of improved diagnostic capability	SSFSE with decreased artifacts without diagnostic impact	Equivalent	vrfSSFSE with decreased artifacts without diagnostic impact	vrfSSFSE with decreased artifacts to the point of improved diagnostic capability
Ability to track pancreatic duct and evaluate for cystic lesions of the pancreas	SSFSE improved to the point of improved diagnostic capability	SSFSE improved without diagnostic impact	Equivalent	vrfSSFSE improved without diagnostic impact	vrfSSFSE improved to the point of improved diagnostic capability
Ability to evaluate cystic lesions of kidneys and evaluate and collecting system	SSFSE improved to the point of improved diagnostic capability	SSFSE improved without diagnostic impact	Equivalent	vrfSSFSE improved without diagnostic impact	vrfSSFSE improved to the point of improved diagnostic capability